Equilibrium properties of superconducting niobium at high magnetic fields: A possible existence of a filamentary state in type-II superconductors

V. Kozhevnikov,[1] A.-M. Valente-Feliciano,[2] P. J. Curran,[3] A. Suter,[4] A. H. Liu,[5] G. Richter,[6] E. Morenzoni,[4]
S. J. Bending,[3] and C. Van Haesendonck[5]

[1]*Tulsa Community College, Tulsa, Oklahoma 74119, USA*
[2]*Thomas Jefferson National Laboratory, Newport News, Virginia 23606, USA*
[3]*University of Bath, Bath BA2 7AY, United Kingdom*
[4]*Paul Scherrer Institut, 5232 Villigen PSI, Switzerland*
[5]*Solid State Physics and Magnetism Section, KU Leuven, BE-3001 Leuven, Belgium*
[6]*Max-Planck-Institut for Intelligent Systems, 70569 Stuttgart, Germany*

The standard interpretation of the phase diagram of type-II superconductors was developed in the 1960s and has since been considered a well-established part of classical superconductivity. However, upon closer examination a number of fundamental issues arises that leads one to question this standard picture. To address these issues we studied equilibrium properties of niobium samples near and above the upper critical field H_{c2} in parallel and perpendicular magnetic fields. The samples investigated were very high quality films and single-crystal disks with the Ginzburg-Landau parameters 0.8 and 1.3, respectively. A range of complementary measurements has been performed, which include dc magnetometry, electrical transport, muon spin rotation spectroscopy, and scanning Hall-probe microscopy. Contrary to the standard scenario, we observed that a superconducting phase is present in the sample bulk above H_{c2} and the field H_{c3} is the same in both parallel and perpendicular fields. Our findings suggest that above H_{c2} the superconducting phase forms filaments parallel to the field regardless of the field orientation. Near H_{c2} the filaments preserve the hexagonal structure of the preceding vortex lattice of the mixed state, and the filament density continuously falls to zero at H_{c3}. Our paper has important implications for the correct interpretation of the properties of type-II superconductors and can be essential for practical applications of these materials.

Interpretation of equilibrium properties of superconductors has a pivotal significance for the entire realm of quantum physics, extending from neutron stars to the standard model [1,2]. Therefore it is important to verify any concerns related to the description of these properties.

Type-II superconductors subjected to a magnetic-field H above the lower critical field H_{c1} can be found in three equilibrium states [3–6]: in the mixed state (MS) where average magnetic induction $\bar{B} < H$ and currents form vortices organized in a hexagonal lattice; in a "surface superconductivity" state, where $B = H$ everywhere except for a sheath with thickness on the order of the Ginzburg-Landau (GL) coherence length near the surface parallel to H; and in the normal state (NS). The typical phase diagram of type-II superconductors of cylindrical geometry (such as, e.g., infinite circular cylinders and slabs with thicknesses greatly exceeding the penetration depth) in the parallel magnetic field or of massive samples with a demagnetizing factor $\eta = 0$ [7] is shown in Fig. 1. Transitions between states, occurring at the critical fields H_{c2} and H_{c3}, are second-order phase transitions. In ellipsoidal samples with $\eta \neq 0$ the sheath forms an equatorial band whose width decreases with increasing η. In samples with $\eta = 1$ (infinite slabs in the perpendicular field) the band vanishes, and surface superconductivity disappears. Since the MS in such samples starts from $H = (1 - \eta)H_{c1} = 0$, their phase diagrams consist of a single curve H_{c2}.

This interpretation of the properties of type-II superconductors is based on two well-known solutions of the linearized GL equation obtained by Abrikosov [8] and Saint-James and de Gennes [9]. Despite a narrow range of applicability of

the GL theory [10–12], its tremendous success has been due to an explanation of the very puzzling properties of these materials.

One of such puzzles was a factor of 2 discrepancy in the upper critical field following from magnetic and resistive measurements. It often was attributed to defects and insufficient sensitivity of magnetometers (see, e.g., Ref. [13]) and therefore ignored in theories (e.g., Ref. [14]). Saint-James and de Gennes treated superconductivity above H_{c2} as an equilibrium property, thus providing an interpretation of the entire phase diagram within one theory.

However this standard picture raises some questions. In particular, it implies that in parallel geometry superconductivity nucleates at a field (H_{c3}) almost twice as large as the field at which it nucleates in perpendicular geometry (H_{c2}). By definition, the field passes the sample in the NS being unperturbed, i.e., not noticing the surface. Hence, nucleation at H_{c3} should not depend on the field-to-surface orientation. Also, in this scenario the states coexisting at H_{c2} belong to different classes of symmetry, such as crystal and liquid. Hence, the phase transition at H_{c2} should not be of second order [15]. In particular, in samples with $\eta = 1$ the coexisting states are the MS and the NS. Apart from different symmetries, the minimum amount of a superconducting (S) phase needed to create the vortex lattice is $\approx$10% of the sample volume. Hence, this transition should not be continuous.

In this paper we challenge the standard interpretation of the phase diagram of type-II superconductors by showing that above H_{c2} the S phase forms filaments parallel to the applied field regardless of its orientation.
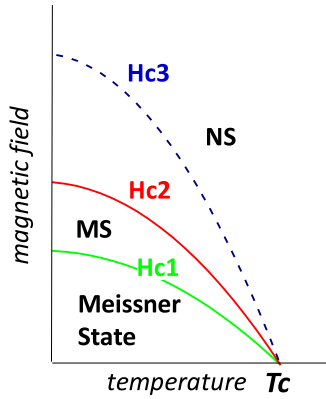
FIG. 1. Phase diagram of a massive type-II superconductor of cylindrical geometry in a parallel magnetic field. MS and NS denote the mixed and the normal states, respectively.

To address the indicated questions, we measured magnetization, electrical transport, and muon spin rotation (μSR) spectra and took scanning Hall-probe microscopy (SHPM) images on Nb samples. Those were two high-purity 5.7-μm-thick films 4×6 mm^2 (Nb-F) and 2×4 mm^2 (Nb-F2) and two one-side polished 1-mm-thick disks with diameters of 7 mm (Nb-SC) and 19 mm (Nb-SC2) cut from the same single-crystal rod. The film samples were cut from a film grown on sapphire using the electron cyclotron resonance technique [16]; its residual resistivity ratio is 640. The GL parameter κ determined from magnetization curves in the parallel field is 0.8 (1.3) near the critical temperature T_c rising up to 1.1 (1.6) at 2 K for the Nb-F (Nb-SC) sample. T_c of the film (single-crystal) samples is 9.25 K (9.20 K). As verified by magnetization measurements, the samples are nearly pinning free at $T \gtrsim 8$ K.

The magnetic moment M was measured on the Nb-F and Nb-SC samples using a Quantum Design magnetic property measurement system. Typical data for high temperatures are shown in Figs. 2(a) and 2(b). We see that H_{c2} and H_{c3} are well distinguishable for both samples. At low temperatures flux trapping is more significant, however it is still possible to resolve the critical fields. An example of the low-temperature data for the Nb-SC sample is shown in Fig. 2(c). We observe that above H_{c2} the S phase is present for both field orientations and in both cases H_{c3} is the same. These results are inconsistent with the surface sheath interpretation. In particular, they suggest that above H_{c2} the S phase forms either droplets or filaments with decreasing number density under an increasing field.

The electrical resistance was measured for the Nb-F2 sample using a low-current (2-mA) ac bridge. The voltage across the potential leads measured vs T at $H = 0$ and vs H at constant T is shown in Fig. 3. In Figs. 3(b) and 3(c) we see that resistance drops abruptly at H_{c3} in the parallel field and at H_{c2} in the perpendicular field, where H_{c2} and H_{c3} are inferred from $M(H)$. This is in line with the data on electrical transport used to support the surface superconductivity interpretation (see, e.g., Refs. [17–20]). However, this interpretation conflicts with the $M(H)$ data. At the same time both resistance and $M(H)$ are consistent with a filament scenario, provided the filaments
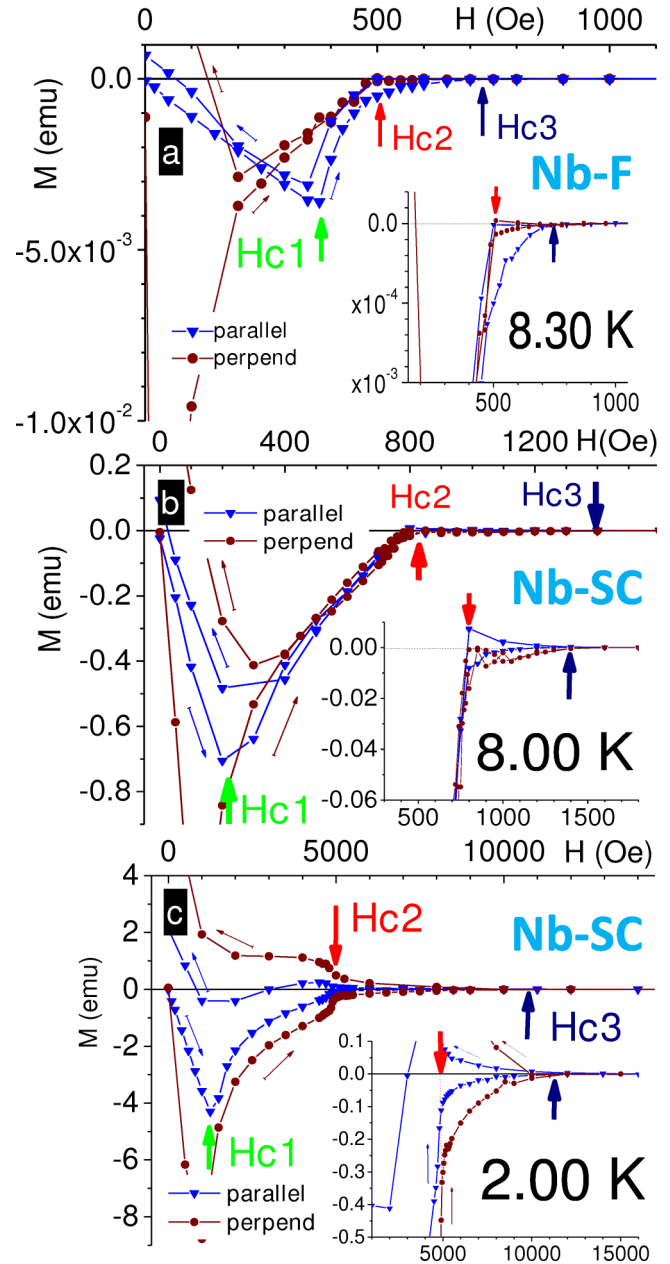
FIG. 2. Magnetic moment of Nb-F and Nb-SC in parallel and perpendicular fields at indicated temperatures. The insets: the same data on an enlarged scale.

are parallel to the applied field. The resistance data rule out the droplet scenario.

Alternatively, magnetic properties can be studied by μSR. Its bulk version makes use of 4-MeV polarized muons, probing B at ~ 0.1 mm below the sample surface, i.e., in the bulk (see, e.g., Refs. [21–23] for details).

μSR spectra were acquired for the Nb-SC2 sample in the perpendicular field at the Dolly instrument of the Swiss Muon Source. The number of events of muon decays collected in each data point is 3×10^6; the statistical error in the measured field is $\lesssim 0.1\%$. Typical time spectra for the MS are shown in Fig. 4(a) where the inset shows the spectra for the NS. For comparison, Fig. 4(b) shows the spectra for the intermediate
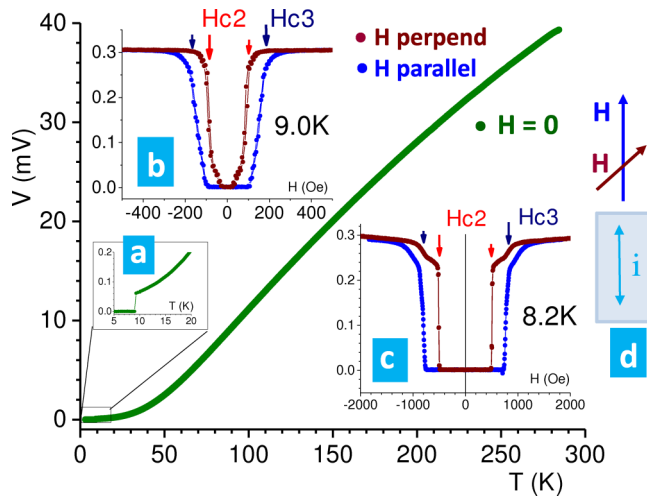
FIG. 3. Voltage V across the Nb-F2 sample. The green dots represent $V(T)$ at $H = 0$; in (a) these data are shown on a magnified scale. (b) and (c) $V(H)$ obtained in parallel (blue dots) and perpendicular (brown dots) fields at indicated temperatures; the red and navy arrows indicate H_{c2} and H_{c3} inferred from the $M(H)$ data, respectively. (d) Current (i) and the field configurations.

state (IS) taken at the same reduced temperature and field for a type-I In sample; the inset shows the spectra of In in the NS.

We see that apart from a much larger damping rate (the damping rate for Nb in the MS normalized relative to that in the NS is greater than the normalized damping rate for In in the IS by a factor of 5), indicating for a strong-field inhomogeneity, the spectra of the MS differ from those of the IS by the absence of the Asy2 [see Fig. 4(b)], caused by nonprecessing muons stopped in S domains with the Meissner ($B = 0$) phase [24]. Unlike the IS, $B \neq 0$ throughout the sample in the MS [5,25]. Therefore, all muons implanted in such samples precess, resulting in the disappearance of Asy2. The absence of Asy2 in μSR spectra of our Nb sample confirms that it is in the MS but not in the intermediate-mixed state [26,27].

Data for the most probable field B_μ extracted from the μSR spectra [22] are shown in Fig. 5 in terms of $\Delta B = B_\mu - H$ vs H on two scales. As seen, $(\partial B_\mu/\partial H)_T$ abruptly changes at H_{c2}. At higher fields ΔB decreases vanishing near H_{c3}. H_{c2} and H_{c3} were inferred from the $M(H)$ data for the Nb-SC sample. The μSR data are consistent with those on magnetization apart from a greater hysteresis under the descending field, probably caused by a stronger pinning in the Nb-SC2 sample. The μSR results confirm the presence of the S phase *in the sample bulk* above H_{c2} *in the perpendicular field*, hence supporting the filament scenario.

Images of the magnetic-field pattern near the surface of the Nb-F sample were taken using a scanning Hall-probe microscope [28]. This was our most challenging experiment due to the low-field contrast and the limited microscope resolution. To maximize the signal-to-noise ratio, the images were taken at the lowest possible fields, i.e., at a temperature (9.20 K) very close to T_c.

Typical images are shown in Fig. 6 where the colors reflect the relative magnitude of the induction and the brightest color
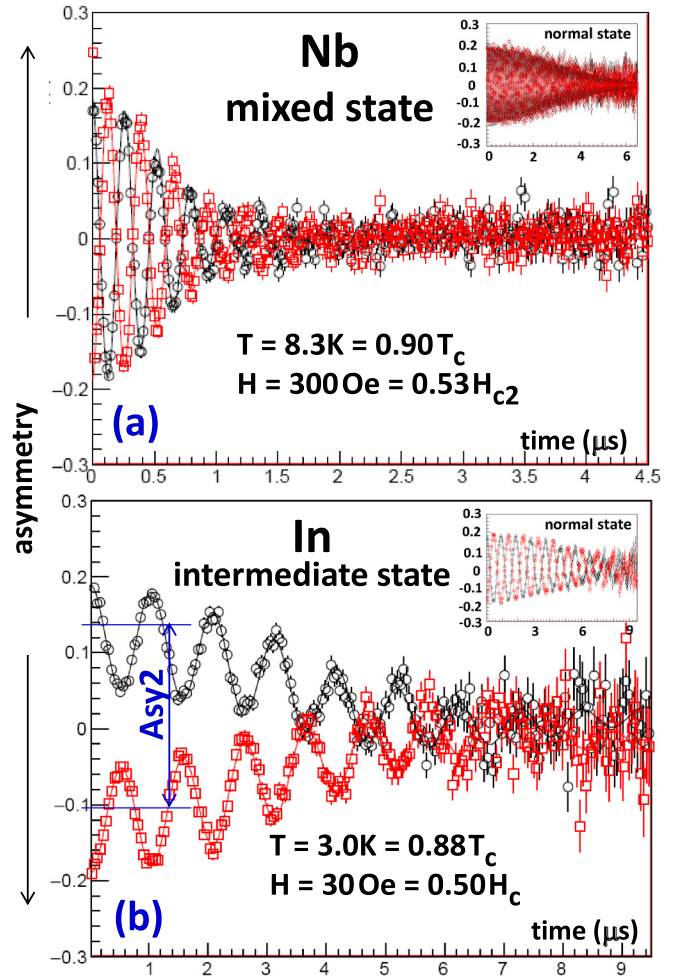
FIG. 4. μSR spectra for (a) single-crystal type-II Nb and (b) single-crystal type-I In at the same reduced temperature and field. The insets show the spectra for the same temperature in the NS. The black (red) dots present the spectra recorded along (opposite to) the initial direction of the muon spin. Asy2 is the asymmetry caused by muons stopping in domains with $B = 0$.

corresponds to the strongest B. We see that, although vortices are clearly distinguishable in a weak field, they become practically unresolvable as H_{c2} is approached. However, a field contrast exceeding the noise level remains below and above H_{c2}. To quantify this observation we calculated $B_{\mathrm{rms}} = \sqrt{\langle (B - \langle B \rangle)^2 \rangle}$, where $\langle \cdots \rangle$ represents a statistical average over the scanned area (7.6×7.6 μm^2). The graphs for $B_{\mathrm{rms}}(H)$ are shown in Fig. 6, where H_{c2} is inferred from $M(H)$. $B_{\mathrm{rms}} \neq 0$ above H_{c2}, and it decreases with increasing H. This agrees with the data on $M(H)$ and $B_\mu(H)$, confirming that the tiny contrast in the SHPM images above H_{c2} is a real feature consistent with the filament interpretation.

We conclude that: (a) All obtained results are in line with each other; (b) the $M(H)$ and μSR data reveal the presence of the S phase above H_{c2} in the perpendicular field at the same field range as in the parallel field; (c) the resistivity data indicate that the S phase forms filaments parallel to the applied field; (d) the filament interpretation is also consistent with the SHPM images.
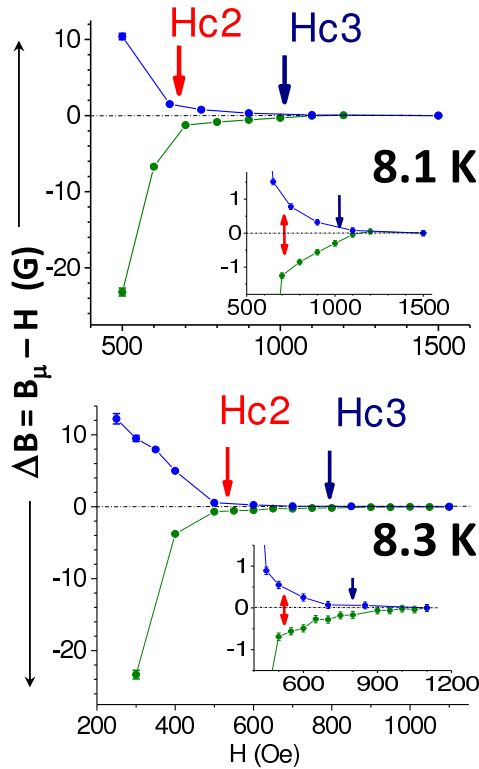
FIG. 5. The difference between the μSR measured B_μ and the applied field H vs H at indicated temperatures. The green (blue) circles are experimental points obtained at the ascending (descending) field. The red and navy arrows indicate H_{c2} and H_{c3} obtained from magnetization measurements.

FIG. 6. Typical SHPM images of the Nb-F sample with numbers indicating the applied field in oersteds. Arrows up (down) indicate images taken at the increasing (decreasing) field. The graph presents $B_{\rm rms}(H)$ obtained from the SHPM data. The red (blue) points represent $B_{\rm rms}$ at the increasing (decreasing) field. The dashed line designates H_{c2} inferred from $M(H)$ data.

Now we turn to the question of what is happening near H_{c2}. First we note that contrary to the IS, where $M(H)$ [29] and $B_\mu(H)$ [24] exhibit strong supercooling at the critical field, in the MS, as seen from Figs. 2 and 5, both $M(H)$ and $B_\mu(H)$ are continuous functions exhibiting discontinuous change in $(\partial M/\partial H)_T$ and $(\partial B_\mu/\partial H)_T$ at H_{c2}. M and B are the first derivatives of the thermodynamic potentials $\tilde{F}_M(T,V,H)$ and $\tilde{F}(T,V,H^i)$, respectively (H^i is the field strength inside the sample) [7]. Therefore our results meet the classical definition of second-order phase transition [30], thus confirming the standard interpretation of the transition at H_{c2}.

Next, since $M(H)$, $B_\mu(T)$ [27] and the heat capacity $C(T)$ [31] are smooth functions in the MS, the equilibrium structure near H_{c2} hardly differs from a periodic lattice of vortices, well verified at low $\bar{B}$ [32]. Therefore the filament structure should also be periodic [15].

Due to hexagonal symmetry of the vortex lattice, a "landscape" of B has "peaks" (vortex cores) with maximum $B = H^i$, "troughs" with minimum B, and "saddle points" between the nearest peaks. Currents form loops about the peaks. The current per unit length of the vortex $g(\varphi,r)$, being a function of the azimuthal (φ) and radial (r) coordinates (see Fig. 7), is determined by the local gradient of the induction $\partial B/\partial r$ [7]. The latter is minimal in the saddle points, thus making these points weak spots in the loops. At H_{c2} the current in the loops ceases. This happens when the angular momentum of electrons in Cooper pairs (or "superconducting electrons")

decreases down to its minimum value, i.e., a quantum of angular momentum $m^* v_r r = \hbar$, where m^* is the effective mass of these electrons and v_r is their speed at radius r. This Bohr's condition yields (see the Appendix) the minimum difference $\delta B_{\rm min}$ between the peaks and the saddle points. In cgs units,

$$\delta B_{\rm min} = \hbar \frac{4\pi n_s e}{c m^*} \ln \frac{R_S}{R_c} = \frac{\Phi_0}{\pi \lambda_L^2} \ln \frac{R_S}{R_c}, \qquad (1)$$
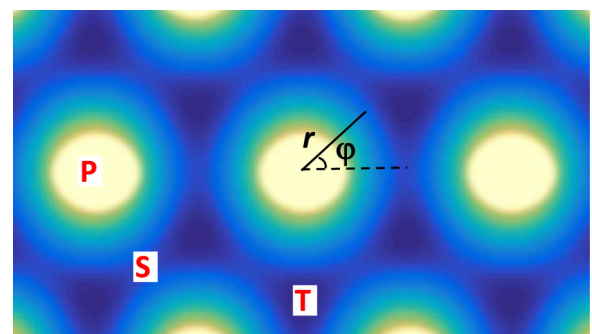
FIG. 7. An induction map of the MS near H_{c2}. The field is perpendicular to the page. P marks the peaks with the highest $B = H^i$, T marks troughs with the lowest B, and S marks the saddle points in between the peaks.

where n_s and e are the number density and charge of the superconducting electrons, λ_L is the London penetration depth, Φ_0 is the flux quantum, R_c is the core radius, and R_S is the radius at the saddle point.

Hence, consistently with Abrikosov [8], one can conclude that at H_{c2} the magnetic landscape is not flat. For instance, if R_S differs from R_c by only 0.01%, $\delta B_{\min}$ is already ~ 1 G. In the troughs B is smaller than in the saddle points, therefore, upon collapse of the vortex current at H_{c2}, the S phase survives at the troughs where it forms filaments in the out-of-plane (parallel to the field) direction. The amount of the S phase just above H_{c2} can be estimated from the difference between the areas of a hexagonal unit cell of the lattice and a circle inscribed in it, which yields about 10% of the sample volume. Currents driven by the field gradient in the troughs now circulate in the filaments. It is important that right above H_{c2} the filaments keep hexagonal symmetry of the vortex lattice below H_{c2}, thus removing the question about impossibility of the second-order phase transition at H_{c2}.

Under increasing H the filaments disappear one by one as it happens with S laminae in the IS [33]. This implies that the filament density continuously decreases down to zero at H_{c3}. This is consistent with the data on M (Fig. 2) and B_μ (Fig. 5).

A final point to be addressed is the nucleation of superconductivity under a decreasing field. One can expect that the first stable nuclei are small droplets in the sample bulk, then the field near the droplets is perturbed, making zones of a depleted field near the droplet poles. Therefore the next nuclei will preferably appear in these zones, thus creating filaments parallel to the field. In such a case the transition at H_{c3} is continuous, in consistency with experiments.

To summarize, results of reported magnetization, electrical transport, μSR, and SHPM measurements performed on Nb samples with different κ's indicate that superconductivity in type-II materials nucleates at H_{c3} regardless of the orientation of the applied field. Between H_{c2} and H_{c3} a superconducting phase exists in the sample bulk, most probably in the form of filaments parallel to the applied field. Under an increasing field above H_{c2} the filament number density decreases vanishing at H_{c3}.

The suggested interpretation of properties of type-II superconductors at a high field is based on experimental results obtained for two low-κ (0.8 and 1.3) superconductors. Therefore it is interesting to verify these observations with materials of higher κ. Single-crystal A15 compounds and high-T_c materials at sufficiently close to T_c temperatures (where pinning is minimal) can be appropriate for such a verification.
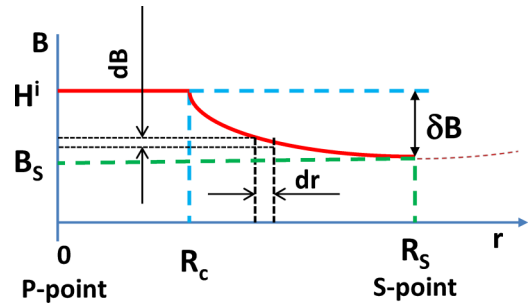
FIG. 8. Profile of induction in a unit cell with a single vortex along the P–S line (see Fig. 7 of the main paper).

APPENDIX: FORMULA (1)

To calculate $\delta B_{\min}$ between the peak and the saddle points at H_{c2} we will use cylindrical coordinates with an axis parallel to **B** with azimuthal φ and radial r coordinates shown in Fig. 7.

The change dB in the normal (radial) direction over a radial interval dr (see Fig. 8) occurs due to the current $dI = l\,dg$ running in the azimuthal direction in the cylindrical layer of radius r and thickness dr, where l is the length of the cylinder (length of the vortex) and g is the current per unit length of the cylinder. In cgs units dB and dg are linked as [7]

$$dB = \frac{4\pi}{c} dg, \tag{A1}$$

where c is the speed of light.

Therefore,

$$dI = l\,dg = l \frac{c}{4\pi} dB = (n_s e v_r) l\,dr, \tag{A2}$$

where n_s, e, and v_r is the number density, charge, and speed of the superconducting electrons (electrons paired in Cooper pairs) in the layer, respectively, and $n_s e v_r$ is the density of the current running through the cross-sectional area $l\,dr$.

Therefore,

$$n_s e v_r r\,dr = \frac{cr\,dB}{4\pi}. \tag{A3}$$

At H_{c2} the Bohr condition for the minimal angular momentum of the superconducting electron is

$$L_{\min} = m^* r v_r = \hbar. \tag{A4}$$

Therefore,

$$dB = \frac{4\pi n_s e(v_r r)}{cr} dr \bigg|_{\text{at } H_{c2}} = \hbar \frac{4\pi n_s e}{crm^*} dr. \tag{A5}$$

Integrating the last expression over the radial interval from the radius of the core R_c to the radius of the saddle-point R_S

one obtains formula (1),

$$\delta B_{\min} = \hbar \frac{4\pi n_s e}{cm^*} \int_{R_c}^{R_S} \frac{dr}{r} = \hbar \frac{4\pi n_s e}{cm^*} \ln \frac{R_S}{R_c} = \frac{\Phi_0}{\pi \lambda_L^2} \ln \frac{R_S}{R_c},$$ (A6)

where Φ_0 and λ_L are the superconducting flux quantum and the London penetration depth, respectively.

---

[1] *Vortices in Unconventional Superconductors and Superfluids*, edited by R. P. Huebener, N. Schopol, and G. E. Volovik (Springer-Verlag, Berlin, 2010).

[2] J. Ranninger, arXiv:1207.6911.

[3] P. G. de Gennes, *Superconductivity of Metals and Alloys* (Westview, Boulder, CO, 1966).

[4] E. M. Lifshitz and L. P. Pitaevskii, *Statistical Physics: Theory of the Condensed State (Course of Theoretical Physics Vol. 9)* (Butterworth-Heinemann Ltd., Oxford, 1980).

[5] A. A. Abrikosov, *Fundamentals of the Theory of Metals* (North-Holland, Amsterdam, 1988).

[6] M. Tinkham, *Introduction to Superconductivity* (Dover Publications, Mineola, NY, 1996).

[7] L. D. Landau, E. M. Lifshitz, and L. P. Pitaevskii, *Electrodynamics of Continuous Media*, 2nd ed. (Elsevier, Amsterdam, 1984).

[8] A. A. Abrikosov, Zh. Eksp. Teor. Fiz. **32**, 1442 (1957).

[9] D. Saint-James and P. G. D. Gennes, Phys. Lett. **7**, 306 (1963).

[10] V. L. Ginzburg and L. D. Landau, Zh. Eksp. Teor. Fiz. **20**, 1064 (1950).

[11] D. Shoenberg, *Superconductivity*, 2nd ed. (Cambridge University Press, Cambridge, UK, 1952).

[12] L. P. Gor'kov, in *100 Years of Superconductivity*, edited by H. Rogalla and P. H. Kes (CRC Press, Boca Raton, FL, 2012), p. 72.

[13] W. F. Druyvesteyn, D. J. Ooijen, and T. J. Berren, Rev. Mod. Phys. **36**, 58 (1964).

[14] M. Tinkham, Phys. Rev. **129**, 2413 (1963).

[15] L. D. Landau and E. M. Lifshitz, *Statistical Physics*, 3rd ed., Part 1 (Elsevier, Amsterdam, 2011).

[16] A.-M. Valente-Feliciano, Development of SRF thin film materials for monolayer/multilayer approach to increase the performance of SRF accelerating structures beyond bulk Nb, Ph.D. Dissertation, Université Paris XI, 2014.

[17] C. F. Hempstead and Y. B. Kim, Phys. Rev. Lett. **12**, 145 (1964).

[18] S. Gygax, J. L. Olsen, and R. H. Kropschot, Phys. Lett. **8**, 228 (1964).

[19] M. Cardona and B. Rosenbblum, Phys. Lett. **8**, 308 (1964).

[20] G. Deutscher, J. Phys. Chem. Solids **28**, 741 (1967).

[21] V. Kozhevnikov, A. Suter, H. Fritzsche, V. Gladilin, A. Volodin, T. Moorkens, M. Trekels, J. Cuppens, B. M. Wojek, T. Prokscha, E. Morenzoni, G. J. Nieuwenhuys, M. J. Van Bael, K. Temst, C. Van Haesendonck, and J. O. Indekeu, Phys. Rev. B **87**, 104508 (2013).

[22] J. E. Sonier, J. H. Brewer, and R. F. Kiefl, Rev. Mod. Phys. **72**, 769 (2000).

[23] A. Yaouanc and P. Dalmas de Reotier, *Muon Spin Rotation, Relaxation, and Resonance* (Oxford University Press, Oxford, 2011).

[24] V. S. Egorov, G. Solt, C. Baines, D. Herlach, and U. Zimmermann, Phis. Rev. B **64**, 024524 (2001).

[25] E. H. Brandt, Phys. Rev. B **68**, 054506 (2003).

[26] M. Laver, E. M. Forgan, S. P. Brown, D. Charalambous, D. Fort, C. Bowell, S. Ramos, R. J. Lycett, D. K. Christen, J. Kohlbrecher, C. D. Dewhurst, and R. Cubitt, Phys. Rev. Lett. **96**, 167002 (2006).

[27] A. Yaouanc, A. Maisuradze, N. Nakai, K. Machida, R. Khasanov, A. Amato, P. K. Biswas, C. Baines, D. Herlach, R. Henes, P. Keppler, and H. Keller, Phys. Rev. B **89**, 184503 (2014).

[28] A. Oral, S. J. Bending, and M. Henini, Appl. Phys. Lett. **69**, 1324 (1996).

[29] V. Kozhevnikov and C. Van Haesendonck, Phys. Rev. B **90**, 104519 (2014).

[30] P. Ehrenfest, Proc. Acad. Sci. Amsterdam **36**, 153 (1933).

[31] B. Serin, in *Superconductivity*, edited by R. D. Parks (Dekker, New York, 1969), Vol. 2.

[32] U. Essmann and H. Trauble, Phys. Lett. A **24**, 526 (1967).

[33] V. Kozhevnikov, R. J. Wijngaarden, J. de Wit, and C. Van Haesendonck, Phys. Rev. B **89**, 100503(R) (2014).